Accepted Manuscript

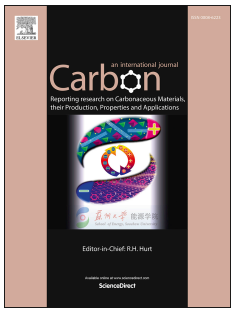

Boosting oxygen reduction and hydrogen evolution at the edge sites of a web-like carbon nanotube-graphene hybrid

Taiwo Odedairo, Xuecheng Yan, Guoping Gao, Xiangdong Yao, Aijun Du, Zhonghua Zhu

PII: S0008-6223(16)30535-8

DOI: 10.1016/j.carbon.2016.06.080

Reference: CARBON 11104

To appear in: *Carbon*

Received Date: 22 March 2016

Revised Date: 3 June 2016

Accepted Date: 22 June 2016

Please cite this article as: T. Odedairo, X. Yan, G. Gao, X. Yao, A. Du, Z. Zhu, Boosting oxygen reduction and hydrogen evolution at the edge sites of a web-like carbon nanotube-graphene hybrid, *Carbon* (2016), doi: 10.1016/j.carbon.2016.06.080.

Boosting oxygen reduction and hydrogen evolution at the edge sites of a web-like carbon nanotube-graphene hybrid

Taiwo Odedairo[a], Xuecheng Yan[b], Guoping Gao[c], Xiangdong Yao[b], Aijun Du[c], Zhonghua Zhu[a,*]

[a]School of Chemical Engineering, The University of Queensland, St Lucia Brisbane Australia.
[b]Queensland Micro- and Nanotechnology Centre, Griffith University, Nathan Campus, Australia.
[c]School of Chemistry, Physics and Mechanical Engineering, Queensland University of Technology, Brisbane Australia.

Abstract

Identifying catalytically active sites in graphene-based catalysts is critical to improved oxygen reduction reaction (ORR) electrocatalysts for fuel-cell applications. To generate abundant active edge sites on graphene-based electrocatalysts for superior electrocatalytic activity, rather than at their basal plane, has been a challenge. *A new type of ORR electrocatalyst produced using fluidization process and based on a three-dimensional hybrid consisting of horizontally-aligned carbon nanotube and graphene (CNT-G), featured abundant active edge sites and a large specific surface area (863 m^2g^{-1}).* The Pt-doped CNT-G exhibited an increase of about 55% in mass activity over the state-of-the-art commercial Pt/C and about 164% over Pt/N-graphene in acidic medium, and approximately 54% increase in kinetic limiting current than the Pt/C at low overpotential in alkaline medium. The higher mass activity indicates that less Pt is required for the same performance, reducing the cost of fuel cell electrocatalyst. *In hydrogen evolution reaction (HER), both the metal-free CNT-G and Pt/CNT-G exhibited superior electrocatalytic activity compared to N-doped graphene and commercial Pt/C, respectively.*

[*]Corresponding author. Fax: +61 73365 4199**.** E-mail address: z.zhu@uq.edu.au (Zhonghua Zhu)

1. Introduction

To reduce the usage of platinum (Pt) in carbon-based electrocatalysts without compromising other electrochemical characteristics is a vital challenge for the commercialization of fuel cells and metal-air batteries [1−5]. Although Pt-based electrocatalysts suffer from sluggish ORR kinetics, low durability, high price and scarcity, they currently remain the most effective catalyst for proton-exchange membrane fuel cells [1,5]. To this end, it is of immense importance to maximize the activity of the Pt-based catalyst by carefully engineering either its morphology or composition.

Known strategies for reducing Pt usage in catalysts include particle size reduction [6], alloying [6−8] and fabrication of suitable supports to promote the reactivity of Pt [9,10]. Two-dimensional materials such as graphene and hexagonal boron nitride offer a variety of outstanding properties which can enhance the performance of Pt-based catalysts via synergistic effects [10−13]. In the case of graphene, its electronic structure, which enables electron transport through either its edge or basal plane, is one of such unique property. The edge sites of graphene are known to exhibit a low contact resistance, which implies faster electron transport at the edges than the basal plane [14−17]. However, previous studies have mainly focused on the ORR enhancement via the basal plane of graphene [11,18−20], with only limited reports on the boosting of ORR via the graphene edge sites [14]. The lack of interest in the utilization of graphene edge sites can be attributed to the previously reported low formation of exposed edge sites on graphene-based catalysts [18,19,21−23], low ORR activity at edge sites of graphene-based catalysts [14] and concerns about the complexity of fabricating porous, graphene-based materials with significantly exposed edge sites. Although progress has been made to fabricate graphite and carbon nanotube (CNT) with significant exposed edges sites using ball-milling [14], these materials still suffer from low porosity/specific surface area, and the ORR performance is still very low.

Herein, we report a new class of ORR electrocatalyst based on a 3D, web-like, horizontally-aligned carbon nanotube-graphene hybrid (CNT-G) with abundant active edge sites and a large ion-accessible surface area, where CNTs are mostly attached to the edges of the graphene, preventing graphene re-stacking [12] and reinforcing the well-developed porous structure. The 3D CNT-G is fabricated by a simple approach in a fluidized-bed microreactor, with plasma as the heat source. This fabrication method is entirely different from the routine plasma system which is not accompanied by a fluidization process but generally associated with a normal surface treatment. The exposed edges of the CNT-G accommodate significant amounts of Pt nanocrystals, a process which exhibits superior ORR performance to that observed for the state-of-the-art commercial Pt/C in both acidic and alkaline media. Relative to the Pt/C and Pt/N-graphene, the as-prepared Pt-doped CNT-G (Pt/CNT-G) exhibited mass ORR activity enhanced 2- and 3-fold, respectively, in an acidic medium. Also, it exhibited an approximately 54% increase in kinetic limiting current compared with the Pt/C at low overpotential in alkaline medium. As a metal-free electrocatalyst, the CNT-G showed higher electrocatalytic hydrogen evolution reaction (HER) activity than the N-doped graphene and exhibited comparable performance to some of the conventional metallic (such as bulk Au and Mo) [24,25] and dual-doped graphene-based catalysts (such as N-P-graphene and C_3N_4/N-doped graphene) [26].

2. Experimental

2.1. Materials

Pt/CNT-G hybrid was prepared via a three-step synthesis approach. *The CNT (outer diameter: < 8 nm, purity: > 95%, length: 10−30 μm and BET surface area: > 350 m^2/g) was purchased from Chengdu Organic Chemicals, China. The CNTs were pre-treated in a mixture of ammonium hydroxide and hydrogen peroxide in a ratio of 50:50 at 100°C for 12 hr in order to preserve the structural integrity of the nanotubes [27]. 20 wt% of the pre-treated carbon nanotube (CNT) was mixed with graphene oxide (GO) slurry (80 wt% GO in water) prepared by a modified Hummers method, sonicated for 30 min and then mixed by a magnetic stirrer for another 5 h at room temperature, followed by a drying process at 30°C.* The dried CNT-coated GO were then reduced in the fluidized-bed microreactor (750 W, 90 sec) with plasma as the heat source, resulting in a volume-expansion ratio of around 85 times; and the expanded products (CNT-G) were collected from the upper-wall of the reactor. *The temperature inside the reactor is about 820°C, determined using an infrared temperature sensor attached to the microwave reactor.* The fluidized-bed microreactor created an environment for an intense upward gas (argon) flow which allowed the unrolling of the reduced graphene oxide from the outer-wall of the CNT. *Finally, CNT-G was impregnated with appropriate amount of H_2PtCl_6, washed with ethanol and de-ionized water several times and then reduced under argon-plasma (250 W, 10 sec) to obtain Pt/CNT-G.*

2.2. Characterization methods

The material morphology was examined by a field emission scanning electron microscope (FE-SEM, JEOL JSM 7100F) and a high resolution transmission electron microscope (HRTEM, JEOL 2100) operating at 200 kV. X-ray photoelectron spectroscopy (XPS) spectra were acquired on a Kratos Axis ULTRA X-ray photoelectron spectrometer. The binding energies were determined using the C 1s line at 284.6 eV from adventitious carbon as a

reference. Recorded spectra were fitted using Gaussian-Lorentzian curves in order to determine the binding energies of the different element core levels more accurately. The Pt content was determined by inductively coupled plasma optical emission spectrometry (ICP-OES, Varian 720-ES). Raman spectra were collected with a Renishaw inVia Raman spectrometer equipped with a Leica DMLM microscope and a 514 nm Ar^+ ion laser as an excitation source. Phase purity of the catalysts was determined by X-ray diffraction in a Bruker Advanced X-ray diffractometer using nickel-filtered Cu Kα X-ray source radiation. The N_2 adsorption measurements of the samples were performed using a Tristar II 3020. See supplementary methods for further details.

2.3. Electrochemical measurements

RDE and RRDE measurements were performed using a CHI Electrochemical Station (Model 760E) in a standard three-electrode cell. A 4.0 mm diameter glassy carbon disk (disk geometric area 0.126 cm^2) was used as the working electrode; a Pt wire and Ag/AgCl (in saturated KCl solution) were used as the counter and reference electrodes, respectively. *The measured potentials versus the Ag/AgCl reference electrode were converted to the reversible hydrogen electrode (RHE) scale via the Nernst equation (see supplementary methods for further details).* Before use, the electrode was polished to mirror flat with alumina powder. The ink formulation is 3 mg of catalyst in a 2.3:1 water-ethanol mixture (1 mL) containing 20 μL of Nafion solution (5 wt%). The ink was shaken and sonicated in bath sonicator for 1 h. 10 μL of catalyst ink was loaded on the electrode surface resulting in a catalyst loading of 0.2389 mg/cm^2. The loading amount of metal for Pt/CNT-G (16 wt% Pt on CNT-G as determined by the ICP-OES) was 38.2 $\mu g/cm^2$, while for the commercial Pt/C (20 wt% Pt Vulcan XC-72) and Pt/N-G (20 wt% Pt on N-G based on ICP-OES measurement), the loading amount of metal was 47.8 $\mu g/cm^2$ based on the geometric electrode area.

3. Results and discussion

3.1. Synthesis of Pt/CNT-G hybrid using a fluidization process

Toxic chemicals are widely used to synthesize graphene-based catalysts, but we employed a facile and eco-friendly fluidized-bed microreactor with plasma as the heat source for scalable production of the 3D web-like horizontally-aligned carbon nanotube-graphene hybrid (CNT-G). By using the fluidized-bed microreactor, it was easy to unroll the reduced graphene oxide from the outer-wall of the CNT during the fluidization process, due to intense upward gas (argon) flow, created through the sample chamber upon placement of the sample in the plasma-zone. Also due to the unique property of the plasma to heat instantaneously [28], reduction of the graphene oxide on the CNT was very fast and without much degradation.

The Pt/CNT-G was prepared via a three-step synthesis as shown in Fig. 1 (see Methods for details). Firstly, the carbon nanotube (CNT)-coated graphene oxide (GO) was prepared by mixing GO slurry with pre-treated CNT, followed by drying (30 °C) (Fig. 1a). We adopted the basic oxidative treatment to completely remove the amorphous carbon and the metal impurities from the CNT in order to keep the structural integrity of the nanotubes intact [27]. We confirmed by inductively coupled plasma optical emission spectrometry (ICP-OES) that the pre-treated CNT contained no iron species (0.01 at%). Secondly, the dried CNT-coated GO were reduced in the fluidized-bed microreactor which is made of a quartz material (750 W, 90 sec), and the CNT-G was collected from the upper-wall of the reactor (Fig. 1b). Finally, CNT-G was impregnated with an appropriate amount of H_2PtCl_6 which was then reduced under argon-plasma (250W, 10 sec) to produce Pt/CNT-G with a Pt content of ~16 wt%, as determined by the ICP-OES. *To identify the optimum composition to generate the unique 3D CNT-G hybrid with abundant edge sites, several composites with varying ratios of CNT to graphene were produced (Table S1).*

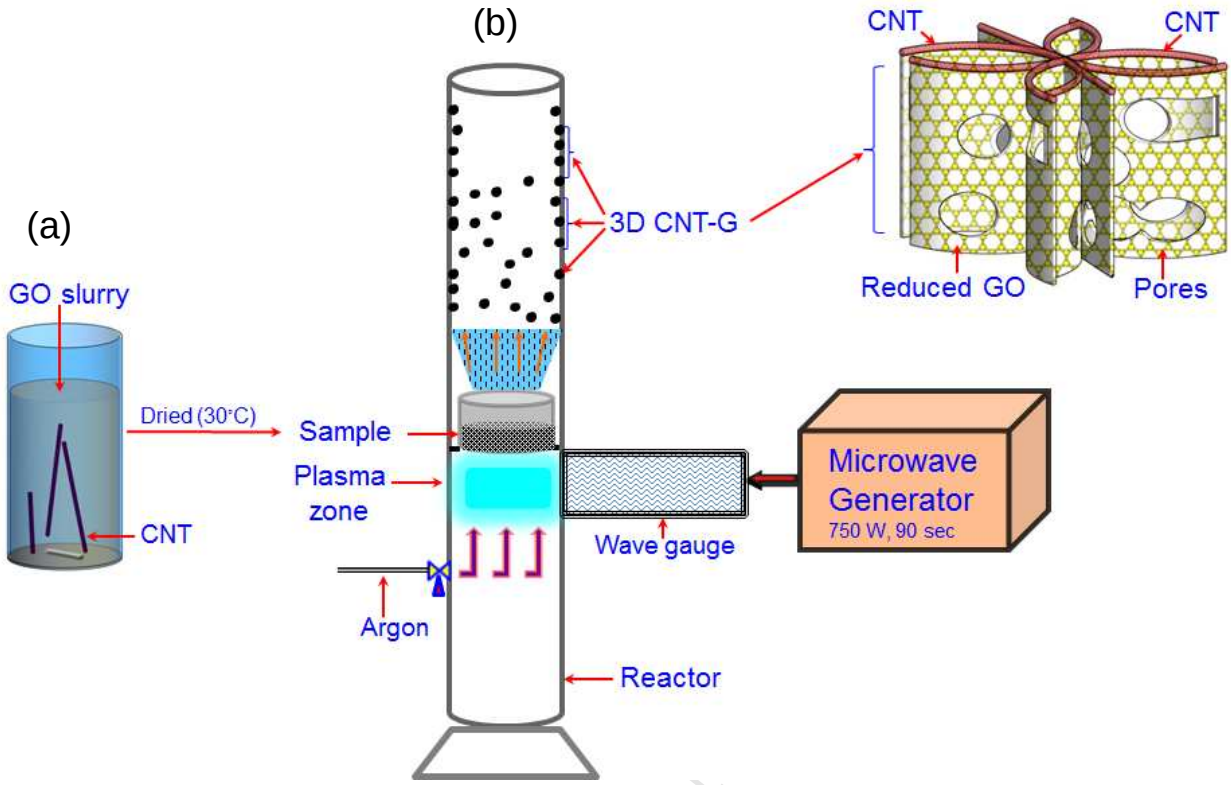

Fig. 1. Schematic of the synthesis of CNT-G hybrid. (a) Sonication and stirring of CNT with graphene oxide (GO) to form CNT-coated GO. (b) Exfoliation of CNT-coated GO in a fluidized-bed microreactor with plasma as the heat source, where GO was reduced to produce the CNT-G.

3.2. Structural characterization of Pt/CNT-G hybrid

Field-emission scanning electron microscopy (FESEM) images (Figs. 2a−c and Supplementary Fig. S1) of the horizontally-aligned carbon nanotube-graphene hybrid (CNT-G) shows a 3D web-like network with a randomly open porous structure. The CNT-G structure exhibits abundant edge sites, with the nanotubes mostly attached to the edges of the graphene sheets, which supresses the stacking of graphene and reinforces the well-developed porous structure. The web-like structure represents a typical morphological feature of the 3D CNT-G synthesized in this work (Figs. 2a−c) and is entirely different from any graphene-based hybrid ever reported, where CNTs are either intercalated vertically or horizontally between the graphene sheets [29,30], or chemical grafted onto the graphene surfaces [22,31].

The CNT-G is formed by the unrolling of the reduced graphene oxide from the outer-wall of the CNT during the reduction process. As a result, CNT-G has a large specific surface area and an ultrahigh pore volume of 863 m^2g^{-1} and 3.3 cm^3g^{-1}, respectively, much higher than that of the reduced graphene oxide (rGO) (527 m^2g^{-1} and 2.5 cm^3g^{-1}) and those of carbon-based composites reported so far, including single-walled carbon nanotube/N-doped rGO (396 m^2g^{-1}) [12] and multiwalled CNT-coated rGO fibre (89 m^2g^{-1}) [31]. The nitrogen adsorption/desorption isotherm of CNT-G has a hysteresis loop, indicating its mesoporous structure (Supplementary Fig. S2).

Figs. 2d, 2e and 3a−c present high-resolution transmission electron microscopy (HRTEM) images of the Pt/CNT-G, while a geometric model showing the interaction that might exist between the CNT and the graphene sheet is shown in Fig. 3d. The HRETM images (Figs. 2d, e and Supplementary Fig. S3) provided the top view of the Pt/CNT-G, confirming the presence of pores and edge sites, where CNTs are horizontally attached to the edges of the graphene sheets with the outer walls of CNT intact and in-line with the FESEM images (Figs. 2a−c and Supplementary Fig. S1). On the other hand, the commercial Pt/C featured no pores with fewer edges (Supplementary Fig. S4).

The HRTEM images reveal the presence of highly dispersed Pt nanocrystals in CNT-G, with an average size of 3.5 ± 0.5 nm. The single Pt nanocrystal at the edge of CNT-G and the corresponding fast Fourier-transform pattern indicate that it was indeed a single crystal with a surface enclosed by {111} facets (Figs. 3b and c). The individual Pt nanocrystals reveal well-defined lattice fringes and an edge lattice spacing of ~0.23 nm (Figs. 3b and c), which is consistent with that expected for face-centered cubic (fcc) Pt.

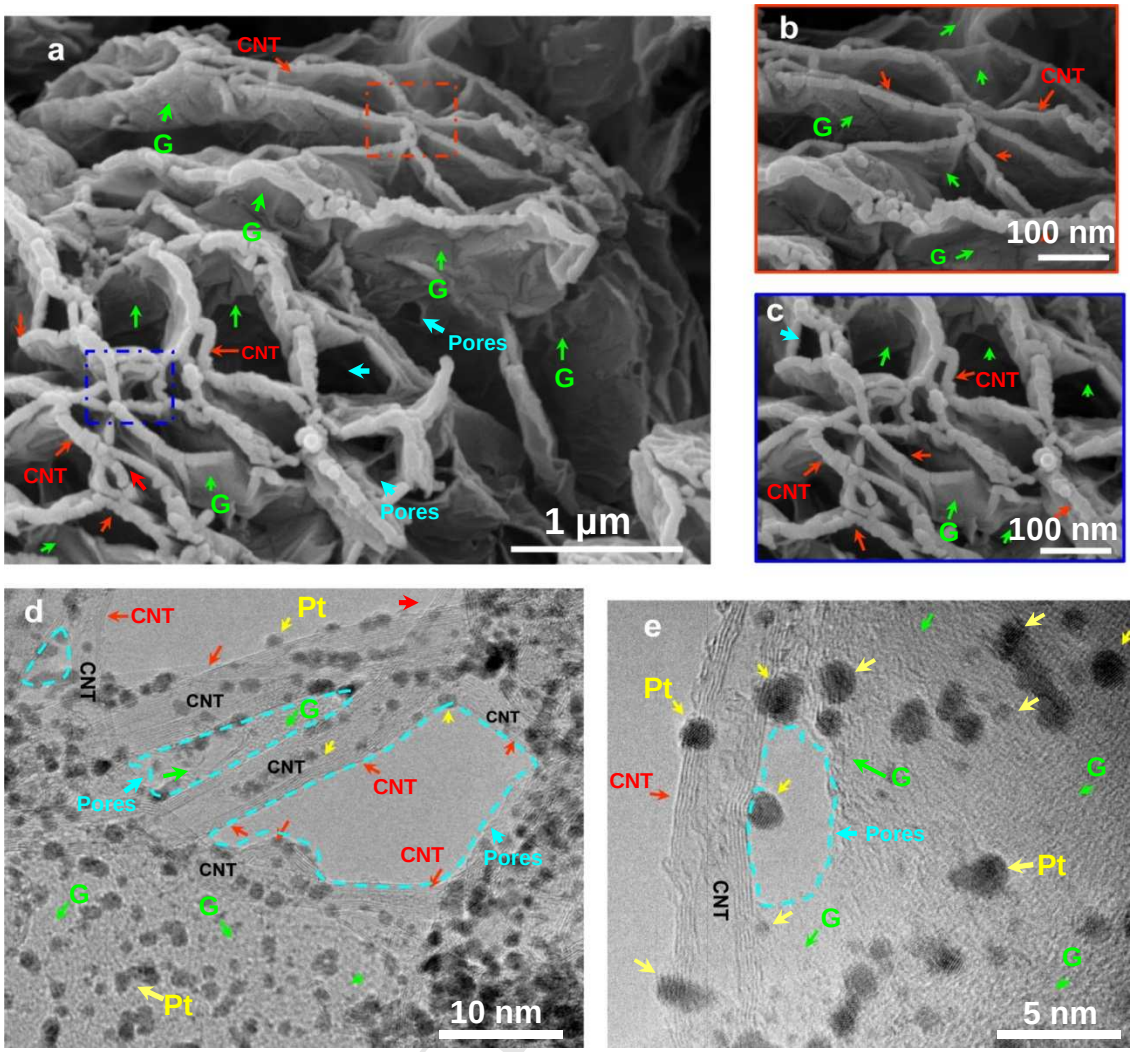

Fig. 2. FESEM and HRTEM images of the CNT-G and Pt/CNT-G. (a−c) FESEM of CNT-G. In (a−c), MWCNTs are shown attached to the edges of the graphene sheet. (d, e) HRTEM of Pt/CNT-G. In d and e, the light-blue highlighted areas represent the pores within the CNT-G hybrid, evident from the FESEM images (a−c). The green, red, yellow and blue arrows designate the graphene sheet, MWCNTs, Pt nanocrystals and pores, respectively.

In order to fully understand the electrocatalytic activity that can be achieved in the experimentally synthesized Pt/CNT-G hybrid, a defective graphene was used to represent the CNT-G with abundant active edge sites and a computational model was built by depositing a Pt_{13} cluster around the edge sites. The geometrical structure is fully relaxed first and then density functional theory (DFT) calculations is performed. We chose Pt_{13} of D_{4h} symmetry, since it is the most energetically favourable structure among the symmetrical isomers [32]. Fig. 3e shows the projected density of states (PDOS) with the corresponding d band centre

(ε_d) of Pt_{13} supported on defective graphene (down) and isolated Pt_{13} (up), representing Pt nanocrystals supported on pristine graphene with few or no edge sites. In our calculation, the ε_d of isolated Pt_{13} cluster (-1.13 eV) is close to Fermi level, while the Pt_{13} cluster supported on defective graphene shows a lower d band centre of -2.17 eV, associated with the strong binding strength of Pt_{13} on the defective graphene[33]. Clearly there is a significant downshift of d-band centre in the Pt/CNT-G. It is well known that the ε_d of the surface metal atom is highly correlated with the binding energy of reactant on metal-containing surfaces [33−35], and has been widely used to design novel catalysts. Normally, a ε_d close to the Fermi level represents strong binding energy, while an ε_d value farther from the Fermi level corresponds to a weak binding energy. Thus, with a lower ε_d value, the Pt_{13} cluster supported on defective graphene can reduce the binding strength of oxygen to a reasonable value and thus significantly promote the ORR kinetics. Therefore, we believe that our unique 3D CNT-G hybrid can be a superior electro-catalyst for ORR, due to the presence of the abundant active edge sites and the resulting large ion-accessible surface area.

Raman spectroscopy was used to determine the edge/defect ratio of N-doped graphene (N-G) and CNT-G. The intensity ratio of D to G bands (I_D/I_G) was used as an indicator of the edge/defect ratio[14]. The intensity ratios of I_D/I_G were about 0.84 and 1.05 for N-G and CNT-G, respectively, suggesting more exposed edges on CNT-G (Supplementary Fig. S5). Fig. 3f shows the XRD patterns of commercial Pt/C and Pt/CNT-G, where peaks of Pt [(111), (200), (220) and (311)] are distinctly observed on both samples, which means that Pt forms the face-centred cubic (fcc) crystal structure. X-ray photoelectron spectroscopy (XPS) showed the presence of Pt, C and O with no other impurity in Pt/CNT-G, while the Pt4f XPS spectra showed that the surface Pt was mainly in the metallic state (Fig. 3g). A positive shift of about 0.5 eV observed for the Pt4f binding energy on Pt/CNT-G in comparison with that of Pt/C (Supplementary Fig. S6), indicates stronger interaction between Pt nanocrystals and CNT-

G[36], which is in line with the expected phenomenon between a metal and a carbon support with significant edge sites [33]. Deconvolution of C1s peaks in Pt/CNT-G, Pt/C and N-G are shown in Fig. 3h and Supplementary Fig. S7, where a main peak at 284.3−285.0 eV is assigned to the graphitic structure. A larger full width at half maximum (FWHM) of the graphitic structure was observed on Pt/CNT-G (1.13 eV) as compared with Pt/C (1.05 eV) and N-G (0.91 eV), confirming presence of more exposed edge sites [37]. Peaks noticed at 285.5 eV can be asigned to defects, while the peaks centred at about 286.5, 287.5, 289.0 and 290.4 eV correspond to the epoxide, C−O, O−C=O and carbonates [22], respectively. The number of defects observed in Pt/CNT-G is ~14.5 at.%, while ~12.6 and 11.1 at.% were observed in Pt/C and N-G, respectively (Fig. 3h and Supplementary Fig. S7), indicating the existence of more edge sites in Pt/CNT-G, in agreement with the FESEM images and Raman spectroscopy analyses (Supplementray Fig. S5).

3.3. Electrocatalytic performance of Pt/CNT-G hybrid

The electrocatalytic oxygen reduction reaction (ORR) properties of as-obtained Pt/CNT-G were measured and compared with the commercial Pt/C (20 wt% Pt on Vulcan XC-72) in both alkaline and acidic mediums. Fig. 4a shows the ORR polarization curves recorded in 0.1 M KOH on a rotating-disk electrode (RDE) with Pt loading of 38.2 μg/cm^2 for Pt/CNT-G and 47.8 μg/cm^2 for the commercial Pt/C and Pt/N-G. *The metal-free CNT-G exhibits superior ORR activity as demonstrated by an $E_{1/2}$ value of ~0.79 V and a current density of ~4.29 mA cm^{-2}, which is much higher than the $E_{1/2}$ (~0.75 V) and current density (~3.11 mA cm^{-2}) noticed on the pristine graphene (Supplementray Fig. S8).* Pt/CNT-G exhibits a half-wave potential ($E_{1/2}$) and an ORR onset potential of ~0.86 and 0.99 V, respectively. The $E_{1/2}$ value of Pt/CNT-G is higher than that of Pt/C (0.85 V) and Pt/N-G (0.83 V) and the ORR onset potential is about 30 mV higher than that of Pt/C (Fig. 4a), indicating higher intrinsic ORR activity [38]. The ORR activity of Pt/CNT-G was further quantitatively evaluated in terms of

kinetic limiting current (J_k) on the basis of the RDE measurments. Remarkably, the J_k value of Pt/CNT-G exceeds that of the Pt/C at 0.85 and 0.90 V vs RHE and was approximately 54% higher than that of commercial Pt/C at 0.90 V (Supplementary Fig. S9). The Pt/CNT-G shows a Tafel slope of 67 mV/decade (Supplementary Fig. S10), which is close to the 63 mV/decade observed in the Pt/C.

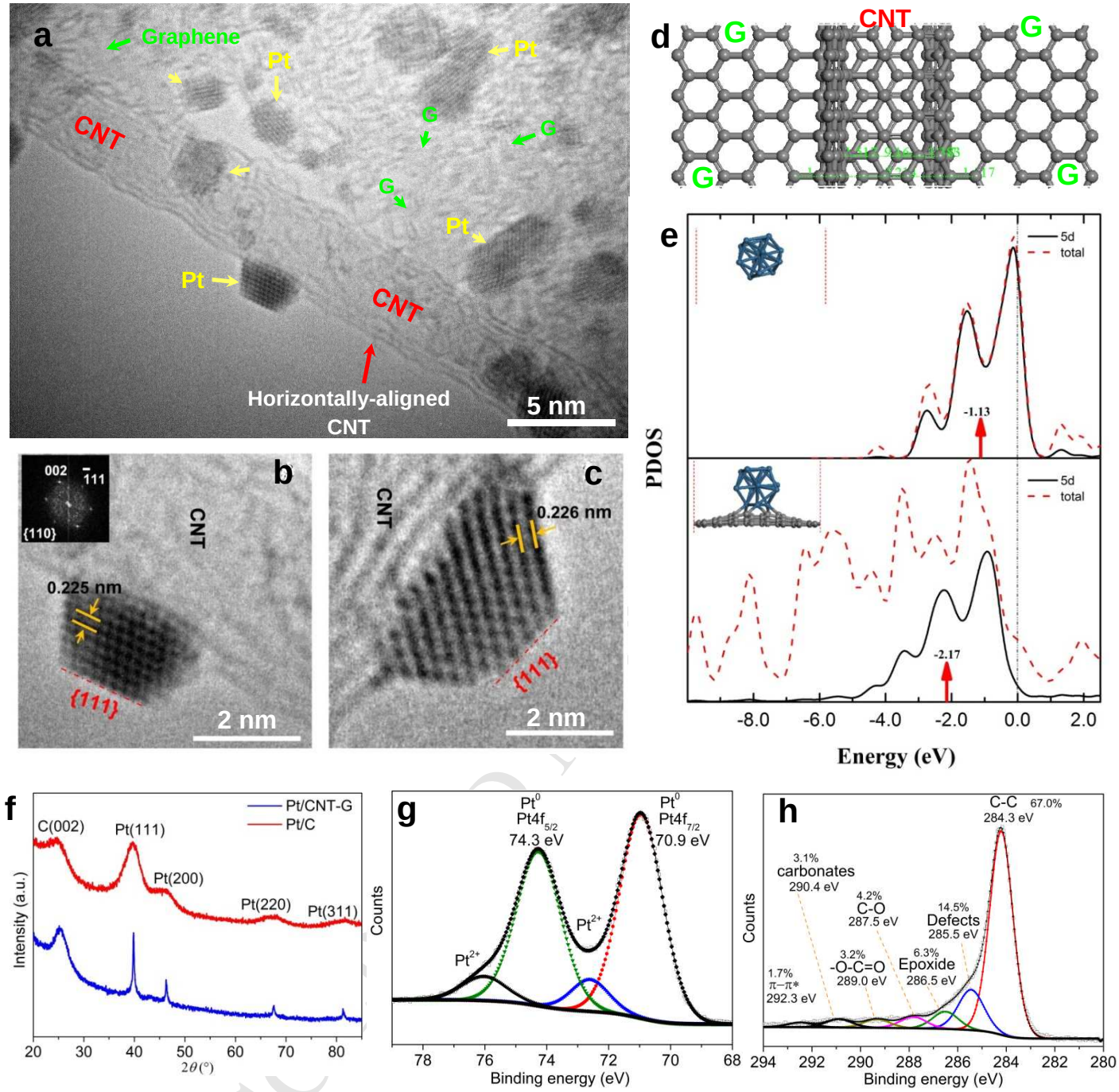

Fig. 3. Structural and compositional characterization of Pt/CNT-G. (a−c) HRTEM images of Pt nanocrystals on CNT-G. In a−c, CNT is attached to the edges of the graphene sheet with Pt crystals loaded on the edges. (d) Geometric model highlighting the interaction between the CNT and the graphene sheet. (e) The projected density of states (PDOS) of isolated Pt_{13} (up) and Pt_{13} (down) supported on defective graphene, while the d band centres are pointed out with red arrows. Colour code: blue-Pt, grey-carbon. (f) XRD of Pt/CNT-G and Pt/C. (g) Pt4f XPS spectra and (h) C1s XPS spectra of Pt/CNT-G catalyst.

The reaction kinetics and number of electrons (*n*) transferred per oxygen molecule in the Pt/CNT-G and Pt/C were evaluated by conducting RDE measurements at different rotating speeds from 400 to 2500 rpm (Supplementary Fig. S11). The electron transfer number can be

calculated based on the Koutecky-Levich (K-L) equation. The *n* value was calculated to be approximately 4.0 at 0.45−0.75 V for Pt/CNT-G from the K-L plot slopes, suggesting a four-electron (4*e*) oxygen reduction process, similar to the Pt/C (n ~4.0 for Pt/C, Supplementary Fig. S12). Rotating ring-disk electrode measurements (RRDE) were performed to confirm the ORR catalytic pathways catalyzed by the samples [23]. The measured peroxide yield is below 3% at all potentials for both Pt/CNT-G and Pt/C, resulting in an average electron transfer number of 3.95 and 3.80 for Pt/CNT-G and Pt/C, respectively (Supplementary Fig. S13), consistent with K-L plots based on the RDE measurements. Chronoamperometric (constant potential) testing confirms very good stability of Pt/CNT-G with about 11% decline in ORR activity over 20000 s of continuous operation, while the Pt/C suffered an activity loss of roughly 21 % (Supplementary Fig. S14). We also investigated the electrochemical durability of both samples by using the U.S. Department of Energy's accelerated durability test protocol, cycling the potential between 0.6 and 1.0 V (vs RHE) [39]. Pt/CNT-G shows a better durability with shift of approximately 15 mV after 5000 cycles as compared with about a 20 mV loss of $E_{1/2}$ observed for Pt/C under the same conditions (Supplementary Fig. S15).

Fig. 4b shows cyclic voltammetry (CV) curves of Pt/C and Pt/CNT-G recorded at room temperature in a N_2-saturated 0.1 M $HClO_4$ solutions at a sweep rate of 50 mV/s. We calculated the electrochemically active surface area (ECSA) by measuring the charge collected in the hydrogen adsorption/desorption region (between 0.05 and 0.35 V) after double-layer correction, and assuming a value of 210 $\mu C/cm^2$ for the adsorption of a hydrogen monolayer [39]. The specific ECSA (the ECSA per unit weigth of metal) of Pt/CNT-G (128.8 m^2/g_{Pt}) was about double that of Pt/C (77.6 m^2/g_{Pt}) and Pt/N-G (71.4 m^2/g_{Pt}) (Fig. 4c), suggesting an increase in the utilization efficiency of Pt. The combination of the highly accessible surface area and the abundant edge sites, should endow the Pt/CNT-G with enhnaced electrocatalytic activity for ORR.

Fig. 4d shows ORR polarization curves for all samples in O_2-saturated 0.1 M $HClO_4$ solution at 10 mV/s at room temperature with a Pt loading of 38.2 μg/cm^2 for Pt/CNT-G and 47.8 μg/cm^2 for the commercial Pt/C and Pt/N-G. It is evident from Fig. 4d that both Pt/C and Pt/CNT-G have similar ORR onset potentials, which are about 27 mV higher than that of Pt/N-G. At low overpotential, the half-wave potential ($E_{1/2}$) of the catalysts increased in the following order: Pt/N-G (0.887) < Pt/C (0.893) < Pt/CNT-G (0.915). The Pt/CNT-G showed a marked positive shift in $E_{1/2}$ of approximately 22 mV relative to Pt/C. These data indicate that Pt/CNT-G exhibits marked activity improvements over Pt/N-G and the state-of-the-art commercial Pt/C.

For better understanding of the mass and surface effects, we normalized the kinetic current calculated from the ORR polarization curves to the Pt mass and ECSA, respectively. As shown in Fig. 4e, the specific activty of Pt/CNT-G was obviously enhanced relative to Pt/C and Pt/N-G, indicating accelerated ORR kinetics on the surface of Pt/CNT-G. The mass activty of Pt/CNT-G was 0.169 mA/μg_{Pt} at 0.9 V versus a reversible hydrogen electrode (RHE), which was 1.6 and 2.7 times greater than that of the commercial Pt/C (0.109 mA/μg_{Pt}) and the Pt/N-G (0.064 mA/μg_{Pt}), respectively (Fig. 4f). The measured ORR activity of the commercial Pt/C was in close agreement with the reported values in the literature [39]. The higher mass activity of the Pt/CNT-G indicates that less Pt is required for the same performance, which would consequently reduce the cost of the fuel cell electrocatalyst. The enhancement in the ORR performance of our Pt/CNT-G could be ascribed to the incremental increase of Pt active sites due to the presence of abundant active edge sites which, in-turn, enhanced faster electron transport.

Chronoamperometric testing confirms very promising performance stability of the Pt/CNT-G with a 22% decay over 10000 s of continuous operation (Supplementary Fig. S16), while the commercial Pt/C suffered a huge activity loss of about 63%, suggesting that the

Pt/CNT-G had a much better stability than the Pt/C. The durability of the catalysts was also evaluated by potential cycling between 0.6 and 1.0 V at 50 mV/s in O_2-saturated 0.1 M $HClO_4$ solution (Supplementary Fig. S17). After 5000 cycles, the Pt/C showed a degradation of about 119 mV in its half-wave potential, $E_{1/2}$, while the degradation of the Pt/CNT-G was much lower, with about a 35 mV negative shift in the half-wave potential, indicating that the Pt/CNT-G was much more durable than the Pt/C. The degradation of Pt/CNT-G in acidic medium is close to the highly active Pt-based bimetallic electrocatalyst (Pt_3Co/C-400) [6], which indicates that Pt/CNT-G might even show better durability if alloyed with a little Co metal. The optimization of synthesis conditions, which is in progress, may lead to a more stable and durable Pt/CNT-G electrocatalyst.

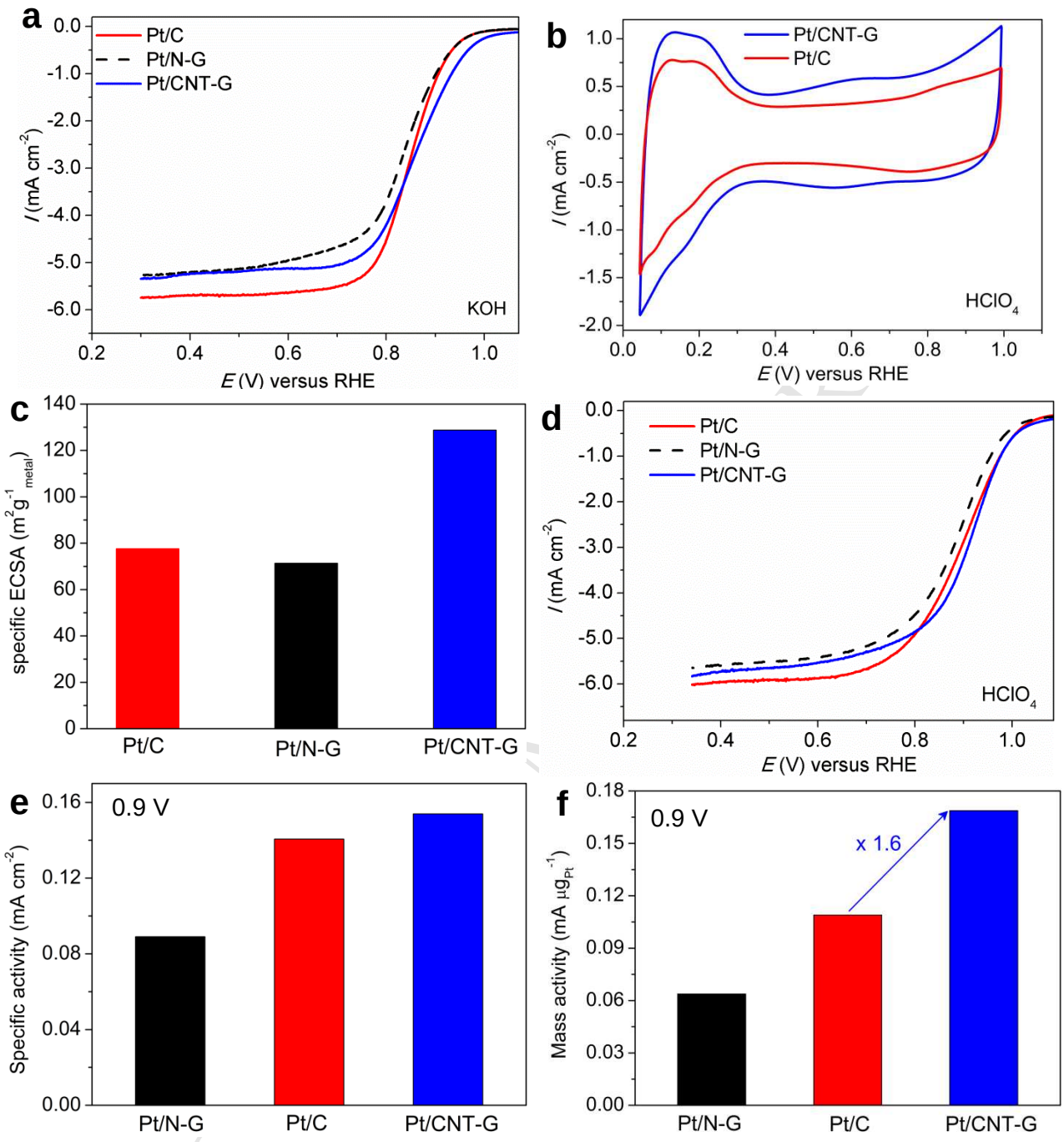

Fig. 4. Comparison of electrocatalytic properties of the Pt/CNT-G, Pt/N-G and Pt/C in ORR. (a) ORR polarization curves for the Pt/C, Pt/N-G and Pt/CNT-G in O_2-saturated 0.1 M KOH solution with a sweep rate of 10 mVs^{-1} and a rotation rate of 1600 rpm. (b) CV curves recorded at room temperature in a N_2-purged 0.1 M $HClO_4$ solution with a sweep rate of 50 mV/s. (c) Specific ECSAs for Pt/C, Pt/N-G and Pt/CNT-G (d) ORR polarization curves for the Pt/C, Pt/N-G and Pt/CNT-G in O_2-saturated 0.1 M $HClO_4$ solution with a sweep rate of 10 mVs^{-1} and a rotation rate of 1600 rpm. (e) Specific activity and (f) mass activity at 0.9 V versus RHE for these three catalysts. Mass and specific activities are given as kinetic current densities normalized in reference to the loading amount and ECSA of metal, respectively. For the Pt/CNT-G, the metal loading was 38.2 $\mu g/cm^2$, whereas the metal loading was 47.8 $\mu g/cm^2$ for the Pt/C and the Pt/N-G.

Since the structural architecture of support plays a crucial role in the efficiency of materials in hydrogen evolution reaction (HER) [30,40], the performance of our as-synthesized CNT-G was investigated as a metal-free electrocatalyst in HER in 0.5 M H_2SO_4 aqueous solution. Fig. 5a shows the polarization curves of the CNT-G and N-doped graphene, used as a reference. To achieve a 10 mA cm^{-2} HER current density, the CNT-G required an overpotential of about 420 mV, lower than that of N-G (~480 mV) and comparable to that of some traditional metallic and metal-free catalysts, such as N-P-graphene [26], C_3N_4/N-doped graphene mixture [41], bulk Au, Mo and Mo/Ni alloy [24,25,42]. The high electrocatalytic HER efficiency of our CNT-G can be ascribed to its hierarchical interconnected structure, which afforded rapid electron transport and also exposed abundant accessible active edge sites that serve as catalytic sites for the HER. As seen in Fig. 5b, both CNT-G and N-G showed Tafel slopes of 89 and 121 mV/decade, respcetively, indicating that an initial proton adsorption was the rate-determining step of the HER process [26,41]. The smaller Tafel slope observed on CNT-G indicates that it requires a lower applied overpotential to generate a required current [43] and signifies better activity in HER. *We also investigated the performance of our Pt/CNT-G in HER, using the commercial Pt/C (20 wt% Pt Vulcan XC-72) as a reference. Strikingly, Pt/CNT-G shows an overpotential of ~37 mV to achieve a 10 mA* cm^{-2} *HER current density, lower than that of commercial Pt/C (~61 mV), in-line with performance of the metal-free CNT-G (Figure 5a). High durability is another vital criteria for a good electrocatalyt. To assess this parameter, the Pt/CNT-G catalyst was cycled contnuously for 1000 cycles. Fig. 5d shows the polarization curves after the* 1000^{th} *cycle with no obvious decay of the activity, suggesting the high catalytic durability of the Pt/CNT-G electrocatalyst.*

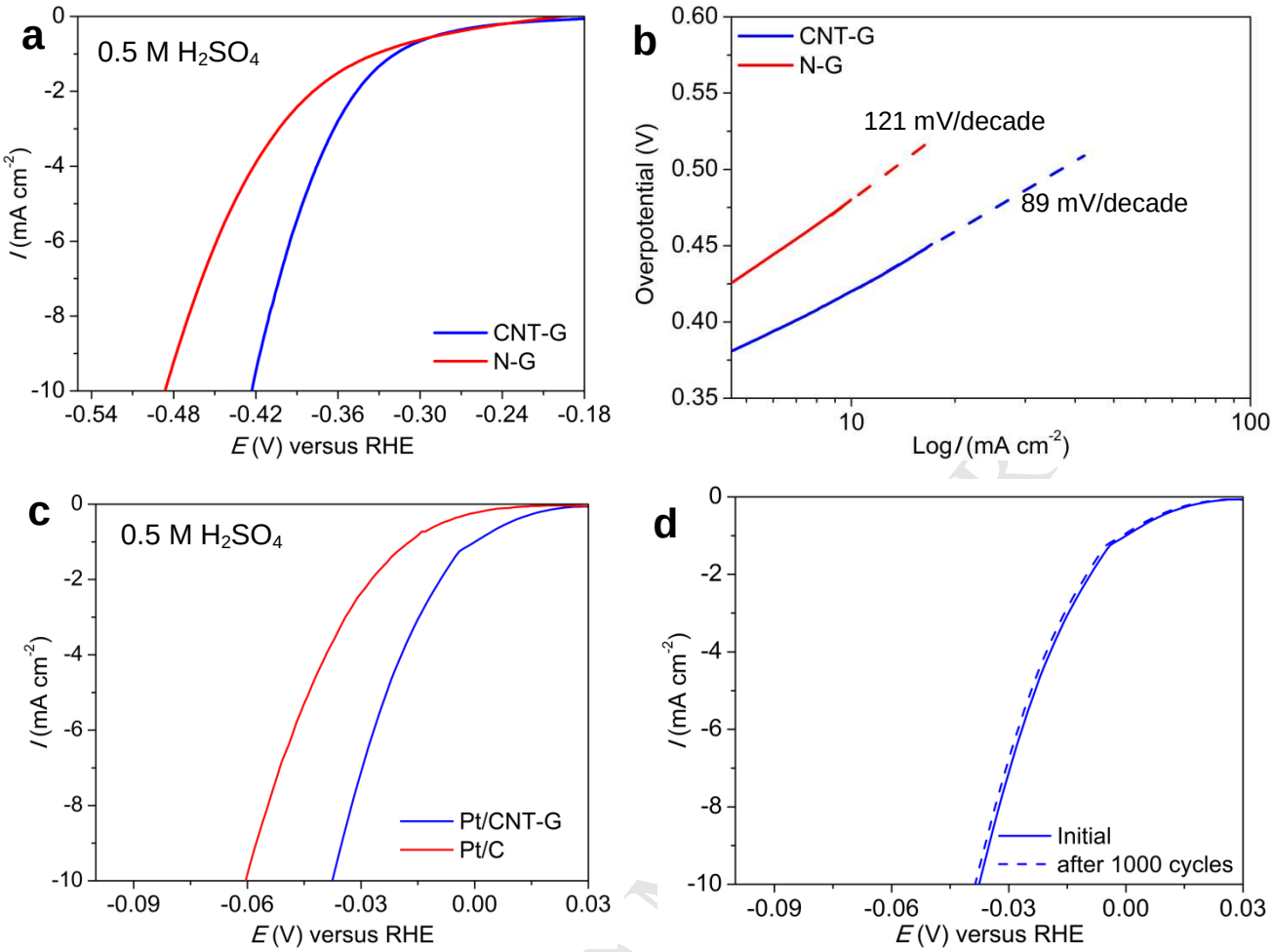

Fig. 5. *Electrochemical evaluation of CNT-G, N-G, Pt/CNT-G and Pt/C as electrocatalysts in HER. (a) The HER polarization curves of CNT-G and N-G, (b) Tafel plots of CNT-G and N-G (c)) The HER polarization curves of Pt/CNT-G and Pt/C in 0.5 M H_2SO_4 with a sweep rate of 10 mVs^{-1}, and (d) Durability test for the Pt/CNT-G hybrid catalyst showing negligible lost after 1000 cycles.*

4. Conclusion

In summary, this work presents a new kind of electrocatalyst for the ORR, composed of a 3D web-like horizontally-aligned carbon nanotube-graphene (CNT-G) hybrid, which features abundant active edge sites, where CNTs are mostly attached to the edges of the graphene, preventing graphene re-stacking and reinforcing the porous structure. We developed a scalable approach to produce the 3D CNT-G hybrid using a fluidization process, with plasma as the heat source. The Pt-doped CNT-G is more active and durable than the state-of-the-art commercial Pt/C in both acidic and alkaline mediums and could represent the next-generation ORR electrocatalyst for fuel-cell applications. *The electrocatalytic HER performance of our metal-free 3D CNT-G is better than the N-doped graphene and comparable to the dual-doped graphene-based catalysts and the traditional metallic catalysts. Also, the Pt/CNT-G exhibited superior HER catalytic performance than the state-of-the-art commercial Pt/C.* Experimental observations in combination with DFT calculations reveal that the unusual electrocatalytic properties of the 3D CNT-G hybrid originate from the abundant active edge sites and the large, ion-accessible surface area, which endows the material with catalytic active sites for both ORR and HER. This study provides a new design stragtegy to generate abundant active edge sites on graphene-based catalysts with both excellent electrocatalytic activity and stability.

References

[1] Y.T. Kim, M.A. Martin, Y.U. Kwon, Graphene as electronic structure modifier of nanostructured Pt film for enhanced methanol oxidation reaction electrocatalysis, Carbon 66 (2014) 691−698.

[2] Z.Z. Lin, Graphdiyne as a promising substrate for stabilizing Pt nanoparticle catalyst, Carbon 86 (2015) 301−309.

[3] J.H. Kim, J.Y. Cheon, T.J. Shin, J.Y. park, S.H. Joo, Effect of surface oxygen functionalization of carbon support on the activity and durability of Pt/C catalysts for the oxygen reduction reaction, Carbon 101 (2016) 449−457.

[4] A.Z. Yazdi, E.P.L. Roberts, U. Sundararaj, Nitrogen/sulfur co-doped helical graphene nanoribbons for efficient oxygen reduction in alkaline and acidic electrolytes, Carbon 100 (2016) 99−108.

[5] M.E.M. Buan, N. Muthuswamy, J.C. walmsley, D. Chen, M. Ronning, Nitrogen-doped carbon nanofibers on expanded graphite as oxygen reduction electrocatalysts, Carbon 101 (2016) 191−202.

[6] D. Wang, H.L. Xin, R. Hovden, H. Wang, Y. Yu, D.A. Muller, F.J. DiSalvo, H.D. Abruna, Structurally ordered intermetallic platinum-cobalt core-shell nanoparticles with enhanced activity and stability as oxygen reduction electrocatalysts, Nat. Mater. 12 (2013) 81–87.

[7] X. Zhao, S. Chen, Z. Fang, J. Ding, W. Sang, Y. Wang, J. Zhao, Z. Peng, J. Zeng, Octahedral Pd@$Pt_{1.8}$Ni core-shell nanocrystals with ultrathin PtNi alloy shells as active catalysts for oxygen reduction reaction, J. Am. Chem. Soc. 137 (2015) 2804–2807.

[8] X. Huang, E. Zhu, Y. Chen, Y. Li, C.Y. Chiu, Y. Xu, Z. Lin, X. Duan, Y. Huang, A facile strategy to Pt_3Ni nanocrystals with highly porous features as an enhanced oxygen reduction reaction catalyst, Adv. Mater. 25 (2013) 2974–2979.

[9] X. Ma, H. Meng, M. Cai, P.K. Shen, Bimetallic carbide nanocomposite enhanced Pt catalyst with high activity and stability for the oxygen reduction reaction, J. Am. Chem. Soc. 134 (2012) 1954–1957.

[10] S.H. Joo, S.J. Choi, I. Oh, J. Kwak, Z. Liu, O. Terasaki, R. Ryoo, Ordered nanoporous array of carbon supporting high dispersions of platinum nanoparticles, Nature 412 (2001) 169−172.

[11] J.N. Tiwari, K. Naath, S. Kumar, R.N. Tiwari, K.C. Kemp, N.H. Le, D.H. Youn, J.S. Lee, K.S. Kim, Stable platinum nanoclusters on genomic DNA-graphene oxide with a high oxygen reduction reaction activity, Nat. Commun. 4 (2013) 2221−2227.

[12] D. Yu, K. Goh, H. Wang, L. Wei, W. Jiang, Q. Zhang, L. Dai, Y. Chen, Scalable synthesis of hierarchically structured carbon nanotube-graphene fibres for capacitive energy storage, Nat. Nanotech. 10 (2014) 555−562.

[13] S. Stankovich, D.A. Dikin, G.H.B. Dommett, K.M. Kohlhaas, E.J. Zimney, E.A. Stach, R.D. Piner, S.T. Nguyen, R.S. Ruoff, Graphene-based composite materials, Nature 442 (2006) 282−286.

[14] A. Shen, Y. Zou, Q. Wang, R.A.W. Dryfe, X. Huang, S. Dou, L. Dai, S. Wang, Oxygen reduction reaction in a droplet on graphite: Direct evidence that the edge is more active than the basal plane, Angew. Chem. Int. Ed. 53 (2014) 10804–10808.

[15] L. Wang, I. Meric, P.Y. Huang, Q. Gao, Y. Gao, H. Tran, T. Taniguchi, K. Watanabe, L.M. Campos, D.A. Muller, J. Guo, P. Kim, J. Hone, K.L. Shepard, C.R. Dean, One-dimensional electrical contact to a two-dimensional material, Science 342 (2013) 614−616.

[16] E.J.H. Lee, K. Balasubramanian, R.T. Weitz, M. Burghard, K. Kern, Contact and edge effects in graphene devices, Nat. Nanotech. 3 (2008) 486−490.

[17] D.W. Yue, C.H. Ra, X.C. Liu, D.Y. Lee, W.J. Yoo, Edge contacts of graphene formed by using a controlled plasma treatment, Nanoscale 7 (2015) 825–831.

[18] Y. Liang, Y. Li, H. Wang, J. Zhou, J. Wang, T. Regier, H. Dai, Co_3O_4 nanocrystals on graphene as a synergistic catalyst for oxygen reduction reaction, Nat. Mater. 10 (2011) 780−786.

[19] Y. Li, W. Zhou, H. Wang, L. Xie, Y. Liang, F. Wei, J.C. Idrobo, S.J. Pennycook, H. Dai, An oxygen reduction electrocatalyst based on carbon nanotube-graphene complexes, Nat. Nanotech. 7 (2012) 394−400.

[20] T. Odedairo, J. Ma, Y. Gu, W. Zhou, J. Jin, X.S. Zhao, Z. Zhu, A new approach to nanoporous graphene sheets via rapid microwave-induced plasma for energy applications, Nanotechnology 25 (2014) 495604−495613.

[21] J. Shui, M. Wang, F. Du, L. Dai, N-doped carbon nanomaterials are durable catalysts for oxygen reduction reaction in acidic fuel cells, Sci. Adv. 1 (2015) e1400129.

[22] T. Odedairo, J. Ma, Y. Gu, J. Chen, X.S. Zhao, Z. Zhu, One-pot synthesis of carbon nanotube-graphene hybrids via syngas production, J. Mater. Chem. A 2 (2014) 1418−1428.

[23] T. Odedairo, X. Yan, J. Ma, Y. Jiao, X. Yao, A. Du, Z. Zhu, Nanosheets Co_3O_4 interleaved with graphene for highly efficient oxygen reduction, ACS Appl. Mater. Interfaces 7 (2015) 21373−21380.

[24] W.F. Chen, K. Sasaki, C. Ma, A.I. Frenkel, N. Marinkovic, J.T. Muckerman, Y. Zhu, R.R. Adzic, Hydrogen-evolution catalysts based on non-noble metal nickel molybdenum nitride nanosheets, Angew. Chem. Int. Ed. 51 (2012) 6131–6135.

[25] W.F. Chen, C.H. Wang, K. Sasaki, N. Marinkovic, W. Xu, J.T. Muckerman, Y. Zhu, R.R. Adzic, Highly active and durable nanostructured molybdenum carbide electrocatalysts for hydrogen production, Energy Environ. Sci. 6 (2013) 943–951.

[26] Y. Zheng, Y. Jiao, L.H. Li, T. Xing, Y. Chen, M. Jaroniec, S.Z. Qiao, Toward design of synergistically active carbon-based catalysts for electrocatalytic hydrogen evolution, ACS Nano 8 (2014) 5290–5296.

[27] V. Datsyuk, M. Kalyva, K. Papagelis, J. Parthenios, D. Tasis, A. Sioku, I. Kallitsis, C. Galiotis, Chemical oxidation of multiwalled carbon nanotubes, Carbon 46 (2008) 833–840.

[28] Q. Zhou, Z. Zhao, Y. Chen, H. Hu, J. Qiu, Low temperature plasma-mediated synthesis of graphene nanosheets for supercapacitors electrodes, J. Mater. Chem. 22 (2012) 6061−6066.

[29] Y. Zhu, L. Li, C. Zhang, G. Casillas, Z. Sun, Z. Yan, G. Ruan, Z. Peng, A.R.O. Raji, C. Kittrel, R.H. Hauge, J.M. Tour, A seamless three-dimensional carbon nanotube graphene hybrid material, Nat. Commun. 3 (2012) 555−562.

[30] S. Peng, L. Li, X. Han, W. Suin, M. Srinivasan, S.G. Mhaisalkar, F. Cheng, Q. Yan, J. Chen, Cobalt nanosheet/graphene/carbon nanotube nanocomposites as flexible electrodes for hydrogen evolution, Angew. Chem. Int. Ed. 53 (2014) 12594–12599.

[31] H. Cheng, Z. Dong, C. Hu, Y. Zhao, Y. Hu, L. Qu, N. Chen, L. Dai, Textile electrodes woven by carbon nanotube/graphene hybrid fibres for flexible electrochemical capacitors, Nanoscale 5 (2013) 3428–3434.

[32] E. Apra, A. Fortunelli, Density functional calculations on platinum nanoclusters: Pt_{13}, Pt_{38}, and Pt_{55}, J. Phys. Chem. A 107 (2003) 2934–2942.

[33] G. Kim, S.H. Jhi, Carbon monoxide-tolerant platinum nanoparticle catalysts on defect-engineering graphene, ACS Nano 5 (2011) 805–810.

[34] B. Hammer, J.K. Norskov, Why gold is the noblest of all the metals. Nature 376 (1995) 238−240.

[35] G. Gao, S. Wei, X. Duan, X. Pan, Influence of charge state on catalytic properties of PtAu (CO) in reduction of SO_2 by CO, Chem. Phys. Lett. 625 (2015) 128−131.

[36] C. Liang, L. Ding, C. Li, M. Pang, D. Su, W. Li, Y. Wang, Nanostructured WC_x/CNTs as highly efficient support of electrocatalysts with low Pt loading for oxygen reduction reaction, Energy Environ. Sci. 3 (2010) 1121–1127.

[37] T.Y. Leung, Determination of the sp^3/sp^2 ratio of C:H by XPS and XAES, J. Non-Cryst. Solids 254 (1999) 156−160.

[38] H.T. Chung, J. H. Won, P. Zelenay, Active and stable carbon nanotube/nanoparticle composites electrocatalysts for oxygen reduction, Nat. Commun. 4 (2013) 1922−1926.

[39] B. Lim, M. Jiang, P.H.C. Camargo, E.C. Cho, J. Tao, X. Lu, Y. Zhu, Y. Xia, Pd-Pt bimetallic nanodendrites with high activity for oxygen reduction, Science 342 (2009) 1302−1305.

[40] Y.H. Chang, C.T. Lin, T.Y. Chen, C.L. Hsu, Y.H. Lee, W. Zhang, K.H. Wei, L.J. Li, Highly efficient electrocatalytic hydrogen production by MoS_x grown on graphene-protected 3D Ni foams, Adv. Mater. 25 (2013) 756–760.

[41] Y. Zheng, Y. Jiao, Y. Zhu, L.H. Li, Y. Han, Y. Chen, A. Du, M. Jaroniec, S.Z. Qiao, Hydrogen evolution by a metal-free electrocatalyst, Nat. Commun. 5 (2014) 3783−3790.

[42] J. Perez, E.R. Gonzalez, H.M. Villullas, Hydrogen evolution reaction on gold single-crystal electrodes in acid solution, J. Phys. Chem. B 102 (1998) 10931–10935.

[43] D. Merki, X.L. Hu, Recent developments of molybdenum and tungsten sulphides as hydrogen evolution catalysts, Energy Environ. Sci. 4 (2011) 3878–3888.

Acknowledgements

The authors acknowledge the facilities and the scientific and technical assistance of the Australian Microscopy and Microanalysis Research Facility at the Centre for Microscopy and Microanalysis, at The University of Queensland. The first author also acknowledges the support from International Postgraduate Research Scholarship (IPRS) and UQ Centennial Scholarship (UQ Cent). Z. Zhu wants to thank the financial support from Australia Research Council Future Fellowship project FT120100720.